

**This is a non-peer reviewed pre-print submitted to EarthArXiv. Subsequent versions of this manuscript may have slightly different content.**

1 Carbon dioxide migration along faults at the Illinois Basin  
2 – Decatur Project revealed using time shift analysis of  
3 seismic monitoring data

4 Idris Bukar<sup>1\*</sup>, Rebecca Bell<sup>1</sup>, Ann Muggeridge<sup>1</sup>, Samuel Krevor<sup>1</sup>

5 <sup>1\*</sup>Department of Earth Science and Engineering, Imperial College London, Royal  
6 School of Mines, London, SW7 2BP, United Kingdom.

7 \*Corresponding author(s). E-mail(s): [i.bukar21@imperial.ac.uk](mailto:i.bukar21@imperial.ac.uk);  
8 Contributing authors: [rebecca.bell@imperial.ac.uk](mailto:rebecca.bell@imperial.ac.uk); [a.muggeridge@imperial.ac.uk](mailto:a.muggeridge@imperial.ac.uk);  
9 [s.krevor@imperial.ac.uk](mailto:s.krevor@imperial.ac.uk);

10 **Abstract**

11 Large scale underground storage of CO<sub>2</sub> is being deployed worldwide to reduce greenhouse gas  
12 emissions to the atmosphere. Modelling studies have investigated the possible risks from the  
13 CO<sub>2</sub> migrating along faults, but this has not yet been observed. We were able to identify such  
14 CO<sub>2</sub> migration at a commercial-scale, demonstration CO<sub>2</sub> storage project, the Illinois Basin -  
15 Decatur Project, including subsequent emergence of the CO<sub>2</sub> into overlying permeable layers.  
16 Our interpretation resolves previous inconsistencies observed at the project and provides a rare  
17 field observation the fluid dynamics of CO<sub>2</sub> moving between faults and reservoir lithology.  
18 The project had deployed time-lapse 3D vertical seismic profile imaging to study CO<sub>2</sub> plume  
19 development, interpreted based on the commonly used amplitude attributes. However, factors  
20 including survey repeatability, subtle seismic fluid effects and irregular filling of the storage  
21 reservoir by CO<sub>2</sub> meant that amplitude anomalies due to CO<sub>2</sub> were not distinct. Here we apply  
22 an alternative interpretation technique to the data based on time shift attributes, resulting in  
23 much clearer plume anomalies. This work provides field validations of previously theorised plume  
24 behaviours and demonstrates the use of an alternative analysis technique to overcome challenges  
25 in interpretation of seismic monitoring data for geological CO<sub>2</sub> storage.

## 26 Introduction

27 Carbon capture and geological storage is being scaled up worldwide to achieve net zero carbon  
28 emissions by 2050 (Krevor et al., 2023; Pörtner et al., 2022). Monitoring CO<sub>2</sub> storage through  
29 time-lapse seismic techniques has provided observations of the flow and trapping behaviour of the  
30 injected CO<sub>2</sub> at storage projects around the world (Furre et al., 2017; Hansen et al., 2013; Ivandic  
31 et al., 2015; Roach & White, 2018). The observations have revealed fluid dynamics which are more  
32 complex and dynamic than analogous subsurface fluids systems due to the properties of CO<sub>2</sub> as a  
33 supercritical fluid at reservoir conditions (Cavanagh & Haszeldine, 2014; Ringrose et al., 2022).

34 Of particular interest is the potential for CO<sub>2</sub> to move buoyantly upwards from a target reservoir  
35 through leakage pathways such as a fault or wellbore, and this has been investigated using geological  
36 analogues, and theoretical and numerical modelling (Gasda et al., 2004; Gilmore et al., 2022; Miocic  
37 et al., 2016; Nordbotten et al., 2009). There are no instances of CO<sub>2</sub> leakage from currently operating  
38 storage projects. However, CO<sub>2</sub> escape from natural subsurface accumulations is observed primarily  
39 through faults, and the escape of hydrocarbon gases through wellbores is pervasive (Dockrill &  
40 Shipton, 2010; Faulkner et al., 2010; Jung et al., 2014; Kang et al., 2016; Miocic et al., 2016;  
41 Onishi et al., 2019). Models of these systems show that complex dynamics emerge depending on the  
42 permeabilities of fault zones relative to reservoir units, and CO<sub>2</sub> migration up leakage pathways can  
43 in some instances be entirely mitigated by trapping as the plume emerges in overlying permeable  
44 strata. Despite their importance, the hydraulic properties of fault zones are notoriously difficult to  
45 evaluate, and there are no engineered settings in which the movement of CO<sub>2</sub> along faults has been  
46 observed.

47 However, while time-lapse seismic surveys provide a means for observation of fluid movement  
48 over time, their acquisition and processing must be performed in a way that maximises repeatability  
49 (Johnston, 2013). In general, land seismic surveys can suffer from significantly more noise than  
50 marine seismic surveys due to scattering by the near surface layer (Stork, 2020). Time-lapse 3D  
51 (i.e. 4D) vertical seismic profile (VSP) surveys at the onshore Illinois Basin – Decatur Project CO<sub>2</sub>  
52 storage site, the focus of this work, were affected by seasonal variations in ground conditions and  
53 source co-location issues due to infrastructure development and permitting difficulties (Couëslan et  
54 al., 2013). The project used an interpretation approach for the 4D data that is based on amplitude  
55 difference (Couëslan et al., 2014) and normalised RMS amplitude difference attributes (Bauer et al.,  
56 2019). The results were ambiguous due to weak time-lapse signals (Couëslan et al., 2013). During

57 the post-injection phase, the project detected an isolated finger of CO<sub>2</sub> in the injection well in a  
58 shallower zone than the injection interval (Zaluski & Lee, 2021), and the lack of seismic monitoring  
59 during that period meant the origins of the CO<sub>2</sub> could not be ascertained.

60 We used time shift attributes to analyse the seismic monitoring data at Decatur, a technique  
61 that has been applied successfully to monitor fluid movement in oil and gas reservoirs (Benguigui  
62 et al., 2012; Falahat et al., 2011; Santos et al., 2016) and to support amplitude interpretation at  
63 CO<sub>2</sub> storage sites (Arts et al., 2004; Chadwick et al., 2004, 2005; Furre et al., 2015; Grude et al.,  
64 2013). The results resolve inconsistencies in the previous interpretation, revealing that the CO<sub>2</sub>  
65 plume at Decatur has been migrating along major faults previously characterised in the reservoir,  
66 and moving in response to injection at a neighbouring site. The analysis thus provides an important  
67 dataset of previously theorised plume migration behaviour between fault zones and reservoir units,  
68 while demonstrating the superiority of a seldom used approach to time-lapse seismic analysis.

## 69 **Results and Discussion**

### 70 **Interpretations of CO<sub>2</sub> plume anomalies from seismic monitoring data**

71 We interpret CO<sub>2</sub> plumes qualitatively from the results of time shift analysis, identifying several  
72 plume layers, with the largest layer in the injection interval (the lower unit of the Mt. Simon A  
73 formation). A second plume layer is identified in the upper unit of the Mt. Simon A formation, and  
74 a third and fourth layer in the Mt. Simon C formation. Figure 1 (a) shows a map view of three  
75 layers located at different depths as interpreted from the first time-lapse monitor. Figures 1 (b) and  
76 (c) show cross sectional views of the plume layers. Also shown are three out of 28 faults interpreted  
77 to transect parts of the Mt. Simon formation. These faults were interpreted prior to injection, from  
78 3D seismic data acquired during site characterisation. Most of the faults have small displacements  
79 relative to the thickness of the Mt. Simon, with the largest vertical displacement estimated to be  
80 about 18 m. All interpreted plume anomalies exceed the lateral coverage of the seismic monitoring  
81 cubes. This is because the VSP surveys employed have a limited imaging aperture given that the  
82 receiver array is located in a well.

83 We check the plume results from our analysis against saturation measurements acquired in the  
84 wells. The seismic results show that layers 1 and 3 should be detected in injection well CCS1, but  
85 not layer 2 which does not reach the well. Observations from the repeat saturation logs confirm this  
86 expectation. However, while monitoring well VW1 shows a detection of an approximately 2 m thick

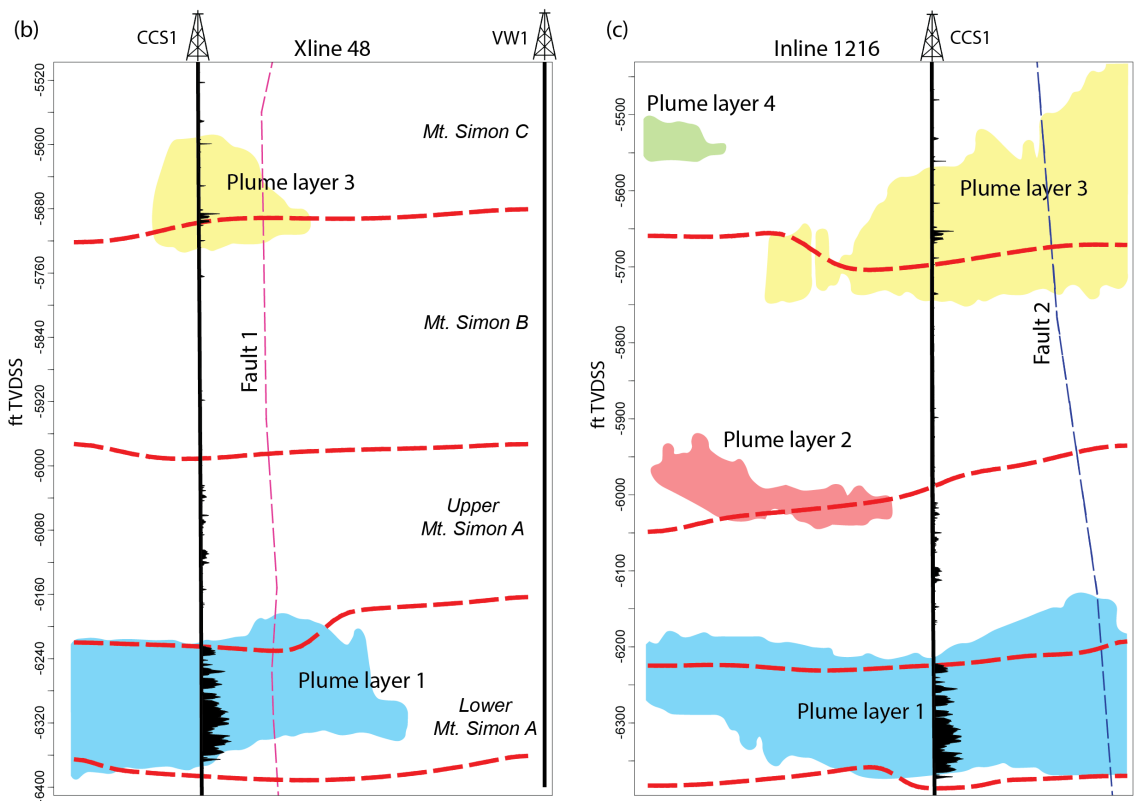
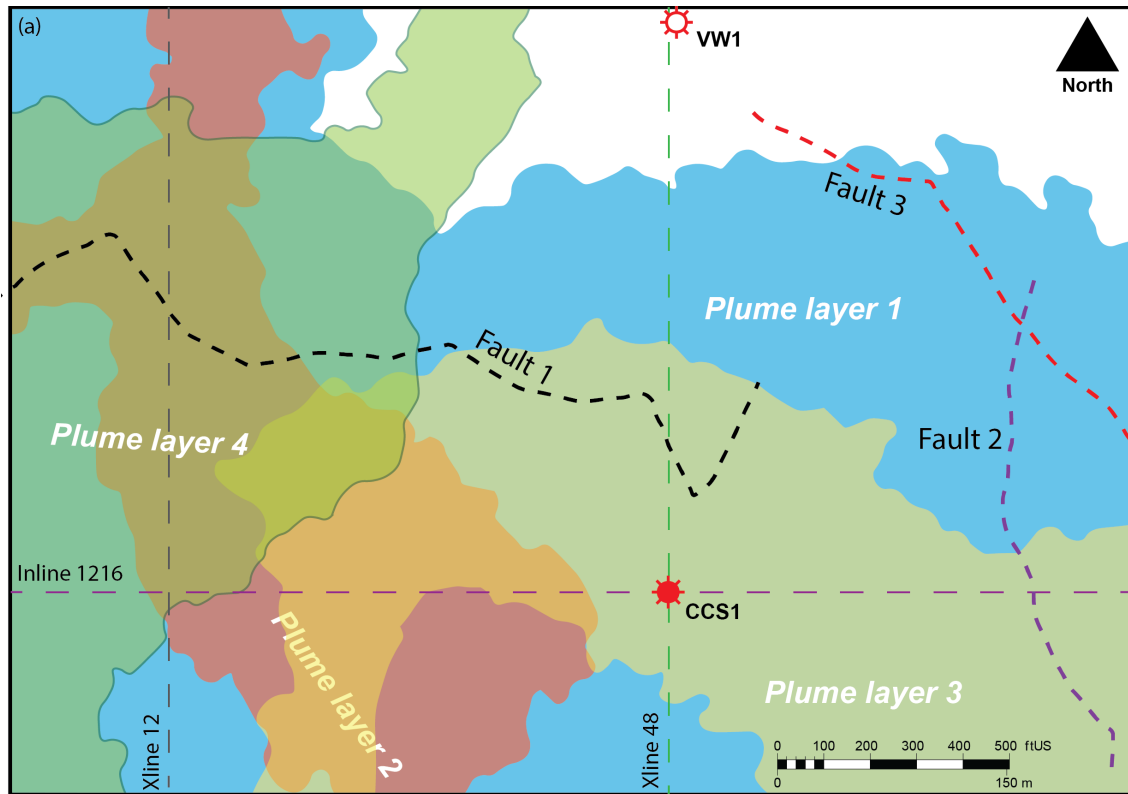


**Fig. 1** (a) A map view of interpreted plume layers from time shift analysis at different depths for the first monitor. (b), (c) Cross sections along the inline and crossline marked in (a). CO<sub>2</sub> saturation from well logging measurements at a time corresponding to the first monitor is shown along the well path. Thicknesses of the upper plume layers appear exaggerated due to the low frequency characteristics of the seismic data.

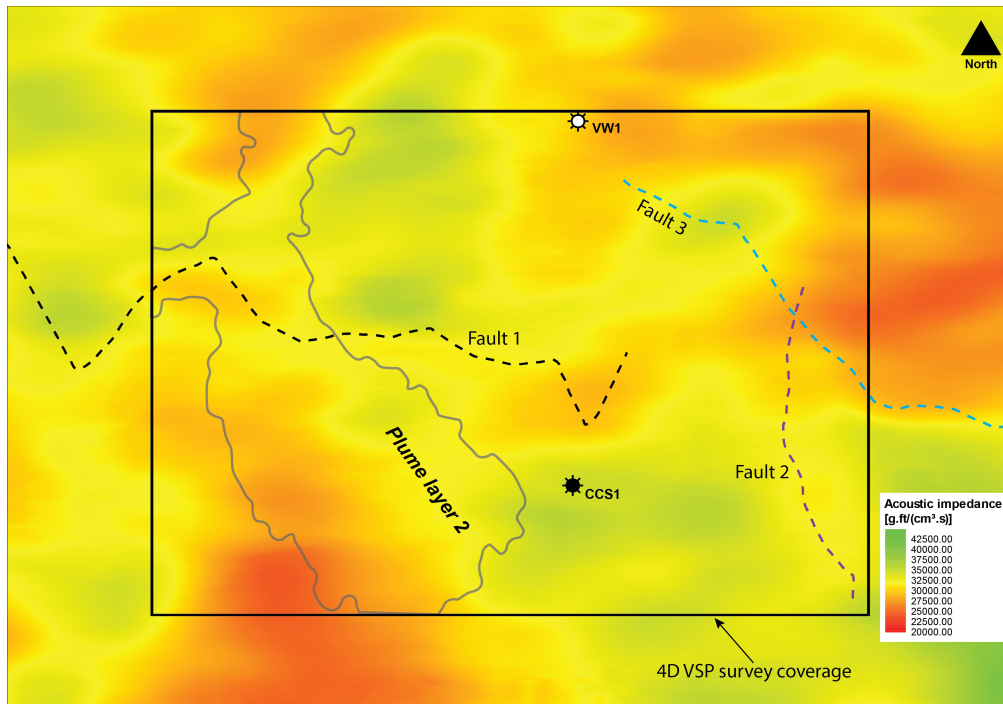


**Fig. 2** Reservoir quality represented by acoustic impedance, with low values (red and yellow) corresponding to high quality regions. Slice shown is at 6000 ft TVDSS. CO<sub>2</sub> plume layer 2 interpreted from 4D VSP within the coverage at the corresponding depth appears to track high quality regions of the reservoir.

87 layer 1 from the saturation log, the interpreted CO<sub>2</sub> plume layer 1 from seismic does not reach the  
 88 well. Given the resolution of the seismic data at the depth of the injection interval of about 20 m, we  
 89 do not expect a 2 m thick plume to be resolved or even detected. Moreover, in the third monitor, by  
 90 which time 730,000 t of CO<sub>2</sub> had been injected and the gross thickness of the plume at VW1 from  
 91 the saturation logs was about 18 m thick, it is detected from the seismic results. The saturation  
 92 logs show that the upper plume layers are thin (layer 3 is about 5 m at the location of well CCS1),  
 93 however, their thicknesses from seismic appear exaggerated due to the low frequency characteristics  
 94 of the data. The plume features from all monitors are qualitatively very similar as observed within  
 95 the narrow monitoring cubes. This suggests that the vertical distribution behaviour, including flow  
 96 through faults, developed quite early, within four months of injection. Therefore, with increasing  
 97 mass of injected CO<sub>2</sub> over time, we expect the major differences to be in the lateral footprint, which  
 98 the narrow cubes make impossible to fully observe.

99 The irregular plume shapes produced by the shallower CO<sub>2</sub> layers appear to be controlled by  
 100 reservoir quality. As shown in Figure 2, the outline of plume layer 2 tracks the high quality regions  
 101 as the CO<sub>2</sub> avoids the poor quality areas. We use a 3D volume of acoustic impedance, a product  
 102 of rock bulk density and P-wave velocity, to represent reservoir quality. Zones of high acoustic

103 impedance represent low quality or tight zones and vice-versa. The acoustic impedance volume was  
104 derived from inversion of 3D seismic data acquired for site characterisation. Acoustic impedance is  
105 a good proxy for reservoir quality in this case because the primary cause of poor reservoir quality  
106 in the upper units of the Mt. Simon is Quartz cementation (Freiburg et al., 2014), which typically  
107 results in higher P-wave velocities by stiffening the rock frame. Cementation also means porosity  
108 destruction, which raises rock bulk densities.

## 109 **Capillary and permeability barriers and vertical CO<sub>2</sub> containment**

110 Early modelling attempts at the Decatur site evaluated the risk of extensive lateral migration as  
111 low and expected a more vertical filling of the lower Mt. Simon sandstone by the injected CO<sub>2</sub>  
112 (Finley et al., 2013). This informed the design of the time-lapse VSP surveys used for studying the  
113 plume development (Couëslan et al., 2009). From observation of the time-lapse saturation logs, it  
114 can be interpreted that contrary to those expectations, the injected CO<sub>2</sub> preferentially fills the high  
115 quality reservoir sandstones and avoids poorer quality or tight sandstones (Figure 3). We define tight  
116 sandstones as those with low porosity, low permeability and high capillary entry pressure. Strandli  
117 and Benson, 2013 and Strandli et al., 2014 show that there is excellent pressure communication  
118 between the two zones where the fingers of the plume are detected in VW1 (zones 2 and 3 in Figure  
119 3), with both bottomhole pressure gauges showing identical behaviours and near-instantaneous  
120 responses to varying injection rates. Nonetheless, the lower finger does not at any point buoyantly  
121 rise and coalesce with the upper finger, even after injection had ceased, as it is held back by a tight  
122 zone at 6294 ft (Figure 3). The upper finger is also contained by another tight zone at 6251 ft. These  
123 tight zones clearly have sufficient permeability to allow good pressure communication across and  
124 even allow the flow of displaced brine as shown by Strandli et al., 2014. This suggests that these  
125 tight zones are capillary barriers rather than permeability barriers.

126 We however do not discount the presence of permeability barriers in the lower Mt. Simon. One  
127 such barrier is a mudstone layer of about 1.8 m thickness at 6182-6186 ft in VW1. Strandli et al.,  
128 2014 show that this layer restricts pressure propagation between zones 2 and 3 below it and zone  
129 4 above it. However, this mudstone layer is discontinuous; it is missing in the injection well and is  
130 penetrated by only two out of the four wells at the site. These mudstones have been interpreted by  
131 Leetaru and Freiburg, 2014 to be interbedded within the Mt. Simon A formation but having a low  
132 preservation potential in an ephemeral fluvial environment. This is evidenced by occasional mudstone  
133 clasts observed in core from well VW1, likely the eroded remnants of the original mudstone deposits

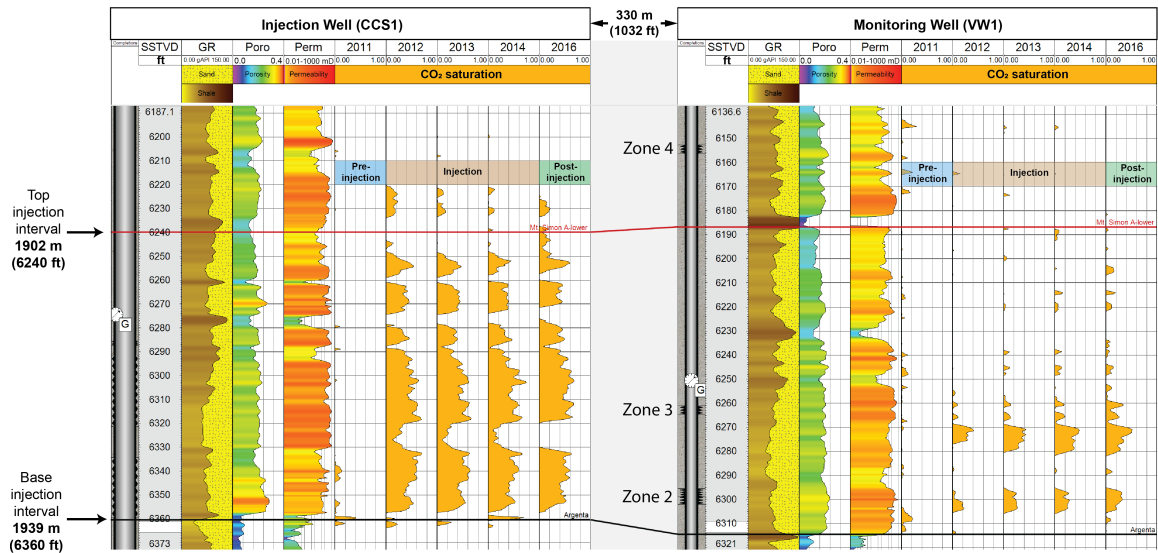


**Fig. 3** Well log panels for the injection and monitoring wells showing reservoir properties and repeat saturation logging measurements from pre-injection, through the injection period to post-injection.

134 (Leetaru & Freiburg, 2014). This is in addition to their complete absence in two wells. Therefore,  
 135 the general vertical containment of CO<sub>2</sub> within the lower unit of the Mt. Simon A formation (the  
 136 injection interval) cannot plausibly be attributed to them.

### 137 CO<sub>2</sub> migration along faults locally within the Mt. Simon and subsequent 138 emergence

139 We interpret CO<sub>2</sub> flow along faults within the Mt. Simon, while it remains contained within high  
 140 quality zones, all below the sealing primary caprock. As shown in Figure 4, the main plume of CO<sub>2</sub>  
 141 in the injection interval is contained within the lower unit of Mt. Simon A. The acoustic impedance  
 142 slice representing reservoir quality shows the lack of high quality pathways through the rock matrix  
 143 for CO<sub>2</sub> to migrate upwards from the injection interval. Saturation logs in CCS1 confirm this as  
 144 they show no continuous CO<sub>2</sub> saturation along the rest of the profile between the detections of layer  
 145 1 and layer 3 (Figure 3). The origin of the CO<sub>2</sub> detected in the overlying zones, therefore, requires  
 146 an alternative explanation. We thus interpret that at least the east-west trending fault 1 shown in  
 147 Figure 1 to be hydraulically conductive and transmitting CO<sub>2</sub> upwards along its apertures under  
 148 gravity, and feeding the upper plume layers from layer 1. Buoyant CO<sub>2</sub> fluid contained within layer  
 149 1 preferentially channels upwards along the fault rather than through the overlying capillary barrier.  
 150 CO<sub>2</sub> entry into the fault implies a lower capillary entry pressure through the fault apertures. We  
 151 propose that CO<sub>2</sub> flows through the fault and emerges when it reaches a point where the reservoir

152 is of high quality, or a point beyond which the fault zone has lower permeability. This is illustrated  
153 in Figure 4.

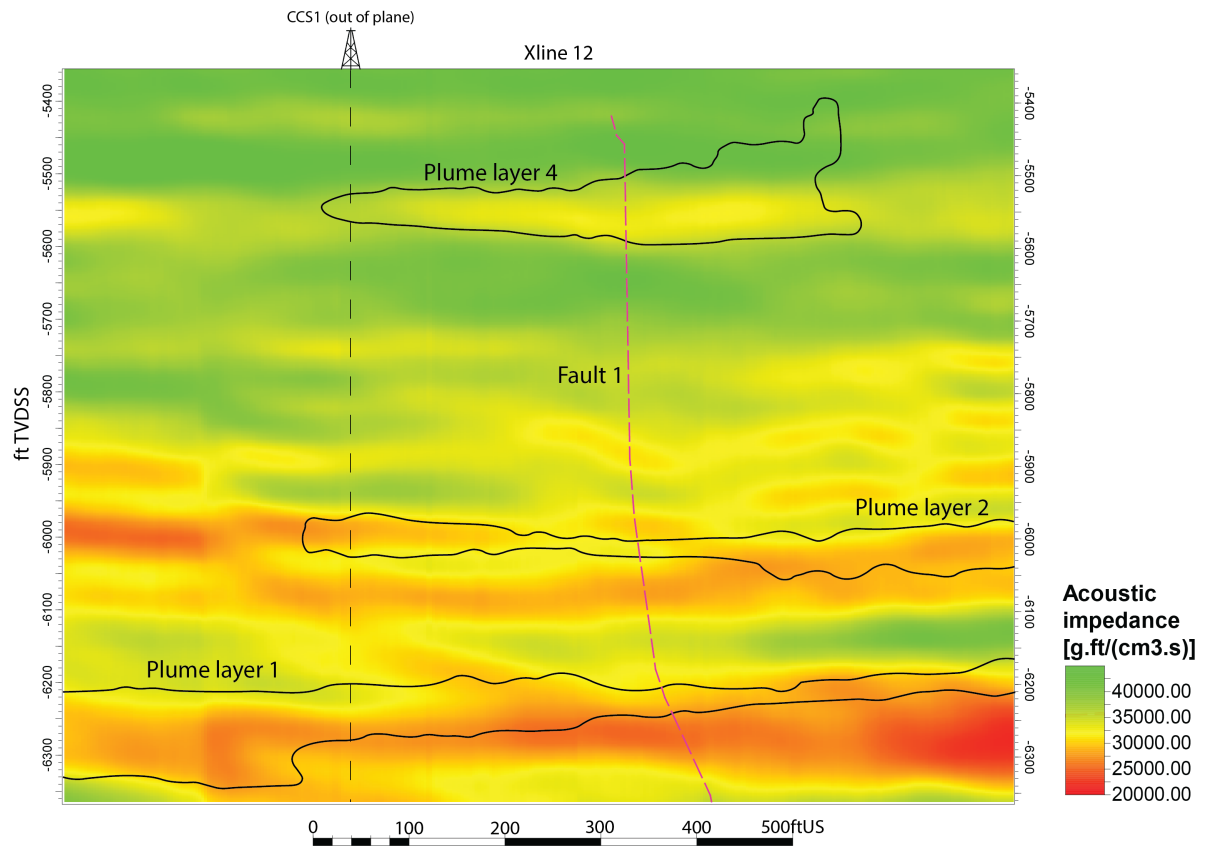


**Fig. 4** Acoustic impedance from 3D seismic inversion used as a proxy for reservoir quality. Interpreted plume outlines are shown to be prevented from buoyantly rising by tight zones or capillary barriers (green regions) and instead channel through permeable faults.

154 We interpret fault 2 and fault 3 (Figure 2) to be non-conductive. This is because we do not detect  
155 the emergence of CO<sub>2</sub> around the faults in the high quality zone at the eastern flank of the monitored  
156 area. This could be because the faults are kept closed by compressive stresses. The Illinois Basin lies  
157 within the east-northeast to west-southwest compressive stress field of the eastern part of the North  
158 American plate, with the maximum horizontal stress orientation ranging between N60°E to N80°E  
159 (Lahann et al., 2017). This could provide a reasonable explanation as to the non-conductive nature  
160 of these faults, which are near perpendicular to the direction of maximum horizontal stress. The  
161 generally east-west trending fault 1, conversely, appears conductive and probably solely responsible  
162 for feeding the overlying plume layers. The behaviour of CO<sub>2</sub> emergence in a high quality zone  
163 could mitigate leakage up conductive faults as the amount of CO<sub>2</sub> that continues to migrate up a



164 fault is progressively reduced with each encountered high quality zone. Where the conductive faults  
165 are intra-reservoir and do not traverse the seal, they would merely serve to provide access to other  
166 good quality zones of the reservoir, distributing the CO<sub>2</sub> among them, as has been shown through  
167 modelling (Yang et al., 2018; Zhang et al., 2024). Such is the case for the Decatur project; the  
168 fault provides flow pathways to overlying good quality zones of the Mt. Simon formation, which the  
169 injected CO<sub>2</sub> is unable to access normally due to capillary barriers.

## 170 **Origins of late CO<sub>2</sub> arrival at injection well post-injection**

171 An isolated finger of CO<sub>2</sub> was detected in the injection well during the post-injection period of the  
172 project in May 2018. This CO<sub>2</sub> was detected in the upper unit of the Mt. Simon A formation, and it  
173 increased in saturation in the March 2019 survey (Figure 5). The saturation logging report (Swager,  
174 2019) suggested the origins of the CO<sub>2</sub> to be the Illinois Industrial Carbon Capture and Storage  
175 project located about 1100 m north of well CCS1. The injection well at this secondary project, well  
176 CCS2, had been injecting into the upper unit of the Mt. Simon A formation for 13 months at the  
177 time of detection.

178 A simplified mass and volume balance analysis shows it is unlikely that enough CO<sub>2</sub> had been  
179 injected in well CCS2 to have reached well CCS1 at the time of detection. We consider flow through  
180 only one-third the thickness of the injection zone at a conservative CO<sub>2</sub> saturation of 0.2 and with  
181 no dissolution. The resulting plume footprint equivalent to 687,000 t of CO<sub>2</sub> that had been injected  
182 at the time is shown in Figure 5 (a). In addition, the uppermost part of the A-Upper unit (c. 5950  
183 ft in well CCS2) has the highest reservoir quality throughout the entire Mt. Simon sandstone, with  
184 permeabilities up to 1000 mD. Given the excellent correlation of this interval across the three wells,  
185 it is the most likely pathway for any rapid migration of CO<sub>2</sub>. However, the late arriving CO<sub>2</sub> was  
186 detected instead in an interval in the lower half of the unit at a depth of 6150 ft. This interval  
187 is deeper than the injection zone in CCS2, which would require the CO<sub>2</sub> to flow downdip. This  
188 is unlikely outside the viscous region due to buoyancy forces. Moreover, no CO<sub>2</sub> was detected in  
189 the corresponding interval of well VW1, which is located between wells CCS2 and CCS1. This is  
190 summarised in Figure 5 (b).

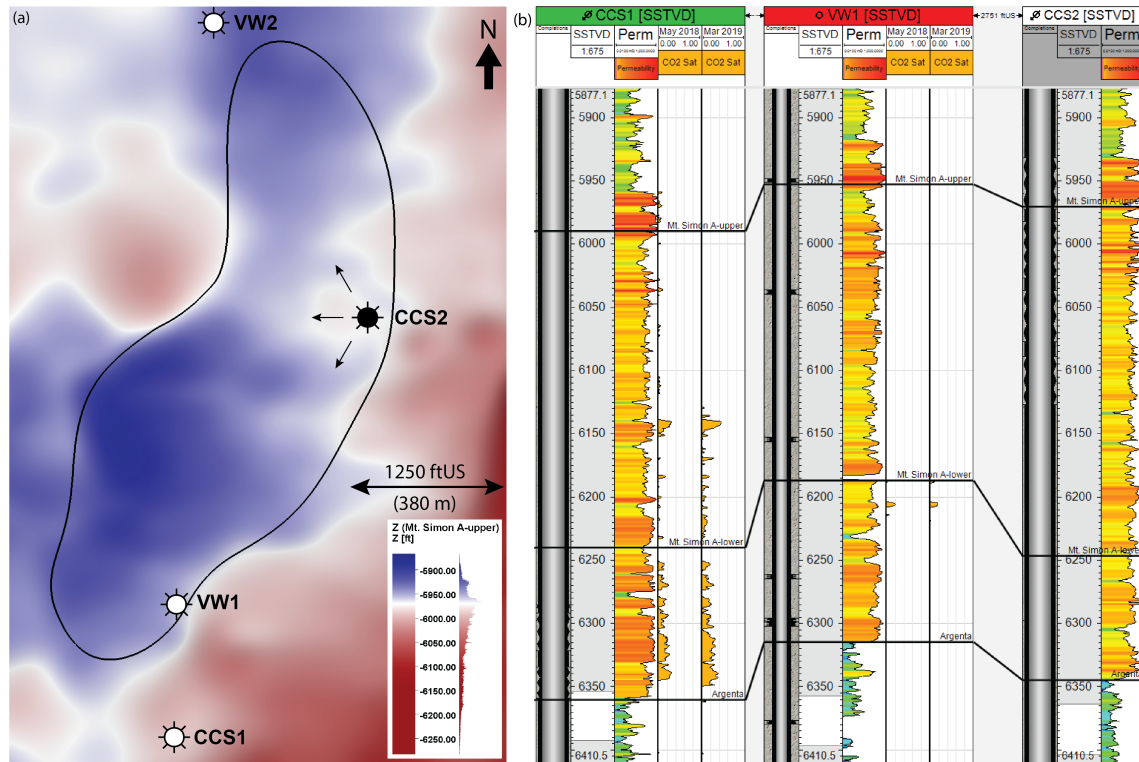


**Fig. 5** (a) CO<sub>2</sub> plume footprint equivalent to 687,000 t of CO<sub>2</sub> derived using a simplified mass and volume balance. (b) Well correlation panel showing wells CCS1, CCS2 and VW1 with no CO<sub>2</sub> detection at VW1.

191 We present an alternative hypothesis based on plume interpretations from seismic time shift  
 192 analysis and pressure and saturation logging data. We propose that the CO<sub>2</sub> instead originated from  
 193 the CCS1 well – the same well it was detected in – but from layer 1 in the underlying injection  
 194 interval. The evidence supports that the CO<sub>2</sub> travelled vertically through Fault 2, forming layer 2  
 195 as shown in Figure 1. Over time, layer 2 got larger as more CO<sub>2</sub> pooled. Once injection began at  
 196 the nearby Illinois Industrial Carbon Capture and Storage project, the pressure gradient induced  
 197 as a result of active CO<sub>2</sub> injection in well CCS2 then forces layer 2 to flow across the face of  
 198 CCS1, resulting in this new detection. We argue this given that bottomhole pressure data shows  
 199 good pressure communication between wells CCS1 and CCS2. Our interpretation of the overall  
 200 CO<sub>2</sub> migration behaviour during the three stages of CCS1 injection, post CCS1 injection and CCS2  
 201 injection is summarised in Figure 6.

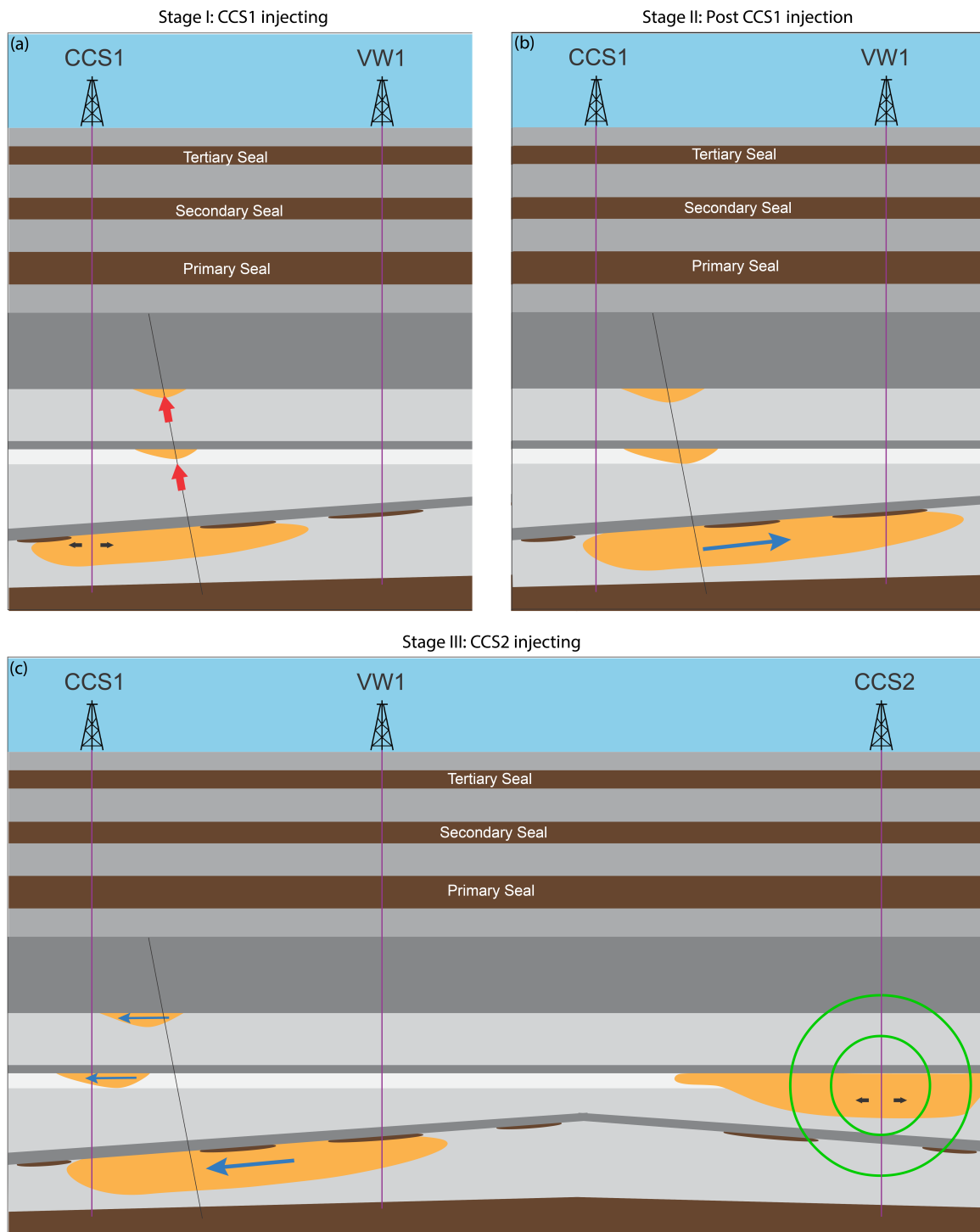


**Fig. 6** A conceptual schematic summarising the overall plume behaviour during (a) CCS injection, (b) post CCS1 injection, and (c) CCS2 injection. Reservoir quality is indicated in grayscale with darker tones representing tight zones.

## 202 **Conclusion**

203 We have re-interpreted data from seismic surveys at the Illinois Decatur Basin Project and shown  
204 that the CO<sub>2</sub> plume has been migrating along major faults between high quality units of the  
205 reservoir, and moving laterally in response to injection at a neighbouring site. The analysis pro-  
206 vides an important dataset of previously theorised plume migration behaviour between fault zones  
207 and reservoir units. This interpretation was otherwise not possible using a conventional analysis  
208 of amplitude attributes. Survey repeatability issues including source point co-location difficulties  
209 and changing ground conditions introduced spurious amplitude anomalies that subtle fluid-related  
210 amplitude anomalies were indistinguishable from. Furthermore, although the lower Mt. Simon reser-  
211 voir is thick, the CO<sub>2</sub> plume does not fill it uniformly and instead forms thin layers that are not fully  
212 resolvable by the seismic data which therefore suffers from tuning of amplitudes. These factors may  
213 occur commonly in projects and are unfavourable to an amplitude-based interpretation, especially in  
214 onshore settings. The much clearer picture of CO<sub>2</sub> plume anomalies provided by time shifts enabled  
215 the overall analysis by allowing a meaningful integration of multiple independent measurements to  
216 produce a coherent interpretation of the migration behaviour of injected CO<sub>2</sub> at the Decatur site.  
217 We were able to identify an interplay of capillary heterogeneity and upward flow of CO<sub>2</sub> along per-  
218 meable faults under buoyancy forces. In addition, we identify the role of pressure gradients resulting  
219 from CO<sub>2</sub> injection at a neighbouring project in causing the re-mobilisation and flow of CO<sub>2</sub> at the  
220 Decatur project post-injection. These behaviours and their impacts have been previously theorised  
221 and the observations provided from an industry scale geological CO<sub>2</sub> storage site provides important  
222 validation of these theories and data from which future projects may be designed.

## 223 **Methods**

### 224 **Monitoring Data from the Illinois Basin - Decatur Project**

225 The Illinois Basin - Decatur Project injected 1 Mt of CO<sub>2</sub> over three years from 2011 to 2014, into  
226 the Mt. Simon sandstone at a depth of c. 2100 m. The Mt. Simon sandstone is a Cambrian-age  
227 saline aquifer and is one of the major CO<sub>2</sub> sequestration resources in the United States. It is over  
228 450 m thick at the Decatur site. Leetaru and Freiburg, [2014](#) and Freiburg et al., [2014](#) provide a  
229 detailed depositional and diagenetic characterisation of it at Decatur. It is unconformably overlain  
230 by the Eau Claire Formation, which is a predominantly shale formation over 90 m thick at the  
231 Decatur site and serves as the primary caprock for the storage unit. The Mt. Simon Sandstone is

subdivided into upper, middle and lower formations. The best reservoir quality occurs in the lower Mt. Simon formation, with porosities of up to 28% and permeabilities of up to 1000 mD, and an average porosity and permeability of 22% and 200 mD. The lower unit of this formation is the injection interval for the project. The project has an injection well (CCS1) and a monitoring well (VW1). Wells CCS2, VW2 are the injection and monitoring wells for the nearby Illinois Industrial Carbon Capture and Storage project. The monitoring data and the data previously acquired for site characterisation form an excellent dataset for studying the complex behaviour of CO<sub>2</sub> plumes in the field. The dataset comprises in-well and geophysical monitoring data including time-lapse 3D VSP surveys. The in-well monitoring data includes bottomhole pressures, injection rates and repeat saturation logs. These logs recorded CO<sub>2</sub> saturation profiles periodically in wells CCS1 and VW1. They provide a time-lapse 1D profile of CO<sub>2</sub> saturation at the high resolution of wireline logging tools. Time-lapse 3D VSP surveying was chosen as the main geophysical monitoring technique to monitor the CO<sub>2</sub> plume in three dimensions. These surveys were meant to provide information on the plume development over time. They were acquired using surface seismic sources with receivers permanently installed in a shallow geophysical monitoring well GM1 located 60 m northwest of the injection well. Surveys were acquired each year from 2012 to 2015, with Baseline 2 being the reference pre-injection survey. Analysis of the time-lapse vertical seismic profile data is the main focus of this work. The survey dates, ground conditions during acquisition and injected CO<sub>2</sub> mass are reported by Couëslan et al., 2013.

## Amplitude and time shift attributes

Previous investigations used amplitude attributes including normalised RMS (NRMS) and amplitude difference (Bauer et al., 2019; Couëslan et al., 2013). We reproduce those analyses by extracting both amplitude difference and NRMS. The attributes do not produce distinct CO<sub>2</sub> plume features as there is a pervasive presence of amplitude anomalies including above the primary seal and below the reservoir in the pre-Cambrian basement. We perform an analysis of time shifts in an attempt to overcome these difficulties in interpretation. Time shifts provide a measure of changes in the two-way travel time of a seismic wave between two surveys, where an increase in travel time results from a slowdown of seismic waves by a lower velocity layer and vice-versa. These time shifts are induced as a result of changes in fluid content or stress leading to compaction or extension in the reservoir or the overburden. Landrø and Stammeijer, 2004 define the relative change in elastic wave travel time due to changes in subsurface layer thicknesses (physical strain) and velocity as  $\frac{\Delta t}{t} = \frac{\Delta z}{z} - \frac{\Delta v}{v}$ , where

263  $\frac{\Delta t}{t}$  is the relative time shift or time strain,  $\frac{\Delta z}{z}$  is the vertical physical strain, and  $\frac{\Delta v}{v}$  is the relative  
 264 velocity change, which is a function of the lithology of the rock and the magnitude of the saturation  
 265 change. For small physical strains, the time strain approximates to  $\frac{\Delta t}{t} = -\frac{\Delta v}{v}$ . Time shifts were  
 266 extracted from full stacks of each of the four 3D monitor surveys relative to the baseline survey.  
 267 MacBeth et al., 2020 provide a review of various methods of measurement of post-stack time-lapse  
 268 time shifts. Dynamic time warping (DTW) algorithm with strain constraints as implemented by  
 269 Hale, 2013 was used to extract the time shifts in this study. It is based on the minimization of the  
 270 dissimilarity error between two traces:  $e[i, q] = (f[i] - g[i + l])^2$ , where  $i$  is the sample index,  $l$  is  
 271 the integer lag or time shift between seismic traces, and  $f$  and  $g$  are the seismic amplitudes of the  
 272 baseline and monitor traces, respectively.

273 The DTW implementation employed imposes constraints on the rate at which shifts may vary in  
 274 time, i.e., a limit on maximum time strain, and this informs the choice of this algorithm. As relative  
 275 velocity change can be approximated to the negative of time strain for small physical strains, we can  
 276 derive from rock physics modelling the maximum saturation change (from available saturation logs),  
 277 which is then used to model the maximum change in rock velocity. This provides constraints on  
 278 the time strain. The rock physics modelling performed involved Gassmann (Gassmann, 1951) fluid  
 279 substitution of brine with CO<sub>2</sub> following a patchy mixing (Brie et al., 1995). The mixing type was  
 280 informed by field observations of velocity-saturation relationships for CO<sub>2</sub> storage in saline aquifers  
 281 (Caspari et al., 2011). Fluid properties at in-situ conditions were computed using the FLAG fluid  
 282 calculator (Han & Batzle, 2014). Constraints on time shifts and relative velocity change can also be  
 283 derived from analogue datasets such as those published in MacBeth et al., 2019. These constraints  
 284 are crucial for the accuracy of the results. Therefore, the atypical availability of the repeat CO<sub>2</sub>  
 285 saturation logs in this dataset was essential to the successful application of this approach.

## 286 Results post-processing and noise removal

287 The obtained time strain volumes were afflicted by noise and artefacts. Most notably, speedup  
 288 anomalies were observed directly beneath the slowdown anomalies. Such artefacts can result from  
 289 data acquisition and processing, and from errors induced in the implementation of the time shift  
 290 algorithms (MacBeth & Izadian, 2023). We removed speedup anomalies ( $\frac{\Delta v}{v} > 0$ ) from the volumes  
 291 as these are normally not expected when CO<sub>2</sub> replaces brine in a reservoir. Nevertheless, residual  
 292 random noise was observed. These are attributed mainly to data acquisition challenges of source  
 293 point co-location and varying ground conditions which may have introduced spurious time shifts in

294 addition to amplitude anomalies throughout the volumes. A noise removal algorithm was developed  
295 to remove the residual noise from the time strain volumes. This relies on the availability of multiple  
296 monitor surveys. It tracks and preserves any features that are consistent across all the monitors,  
297 while discarding any non-consistent features. The design of this filter is based on an assumption that  
298 real plume anomalies would be consistent across the surveys while random noise would not. This is  
299 supported by the observed CO<sub>2</sub> plume distributions at well locations which remain largely the same  
300 over the injection period. Points of consistency in anomalies across all the monitors are identified as  
301 seed points, and the noise filter is applied, where the anomalies grow laterally and upwards starting  
302 from those seed points. This algorithm is based on the image segmentation algorithm of Flood Fill,  
303 and in this case effectively mimics the actual growth of the plume.

## 304 Data availability

305 The original dataset used in this study was made publicly available by the National Energy Tech-  
306 nology Laboratory through the Energy Data eXchange, available at [https://doi.org/10.18141/](https://doi.org/10.18141/1854142)  
307 [1854142](https://doi.org/10.18141/1854142).

## 308 Acknowledgments

309 The authors wish to acknowledge support from SLB and Ikon Science for academic licenses for Petrel  
310 and RokDoc. We thank the Petroleum Technology Development Fund for providing the funding for  
311 this research.

## 312 References

- 313 Arts, R., Eiken, O., Chadwick, A., Zweigel, P., Van der Meer, L., & Zinszner, B. (2004). Monitoring  
314 of CO<sub>2</sub> injected at Sleipner using time-lapse seismic data [Publisher: Elsevier]. *Energy*,  
315 *29*(9-10), 1383–1392.
- 316 Bauer, R., Will, R., Greenberg, S. E., & Whittaker, S. G. (2019). Illinois basin–Decatur project. In  
317 *Geophysics and geosequestration* (pp. 339–369). Cambridge University Press.
- 318 Benguigui, A., Roberts, G., & Shaw-Champion, M. (2012). Time-lapse 2D seismic steamflood  
319 monitoring-a case study from offshore republic of Congo, the Emeraude field. *74th EAGE*  
320 *Conference and Exhibition incorporating EUROPEC 2012*, cp–293.

- 321 Brie, A., Pampuri, F., Marsala, A., & Meazza, O. (1995). Shear sonic interpretation in gas-bearing  
322 sands. *SPE Annual Technical Conference and Exhibition?*, SPE-30595.
- 323 Caspari, E., Müller, T. M., & Gurevich, B. (2011). Time-lapse sonic logs reveal patchy CO2 sat-  
324 uration in-situ [eprint: <https://onlinelibrary.wiley.com/doi/pdf/10.1029/2011GL046959>].  
325 *Geophysical Research Letters*, 38(13). <https://doi.org/10.1029/2011GL046959>
- 326 Cavanagh, A. J., & Haszeldine, S. (2014). The Sleipner storage site: Capillary flow modeling of a  
327 layered CO2 plume requires fractured shale barriers within the Utsira Formation [Publisher:  
328 Elsevier]. *International Journal of Greenhouse Gas Control*, 21, 101–112.
- 329 Chadwick, R., Arts, R., & Eiken, O. (2005). 4D seismic quantification of a growing CO2 plume at  
330 Sleipner, North Sea [Issue: 1]. *Geological Society, London, Petroleum Geology Conference*  
331 *series*, 6, 1385–1399.
- 332 Chadwick, R., Arts, R., Eiken, O., Kirby, G., Lindeberg, E., & Zweigel, P. (2004). 4D seismic  
333 imaging of an injected CO2 plume at the Sleipner Field, Central North Sea [Publisher: The  
334 Geological Society of London]. *Geological Society, London, Memoirs*, 29(1), 311–320.
- 335 Couëslan, M. L., Ali, S., Campbell, A., Nutt, W., Leaney, W., Finley, R., & Greenberg, S.  
336 (2013). Monitoring CO2 injection for carbon capture and storage using time-lapse 3D VSPs  
337 [Publisher: Society of Exploration Geophysicists]. *The Leading Edge*, 32(10), 1268–1276.
- 338 Couëslan, M. L., Butsch, R., Will, R., & Locke II, R. A. (2014). Integrated reservoir monitoring at  
339 the Illinois Basin–Decatur Project [Publisher: Elsevier]. *Energy Procedia*, 63, 2836–2847.
- 340 Couëslan, M. L., Leetaru, H. E., Brice, T., Leaney, W. S., & McBride, J. H. (2009). Designing a  
341 seismic program for an industrial CCS site: Trials and tribulations [Publisher: Elsevier].  
342 *Energy Procedia*, 1(1), 2193–2200.
- 343 Dockrill, B., & Shipton, Z. K. (2010). Structural controls on leakage from a natural co2 geologic  
344 storage site: Central utah, usa. *Journal of Structural Geology*, 32(11), 1768–1782.
- 345 Falahat, R., Shams, A., & MacBeth, C. (2011). Towards quantitative evaluation of gas injection using  
346 time-lapse seismic data [Publisher: European Association of Geoscientists & Engineers].  
347 *Geophysical Prospecting*, 59(2), 310–322.
- 348 Faulkner, D., Jackson, C., Lunn, R., Schlische, R., Shipton, Z., Wibberley, C., & Withjack, M.  
349 (2010). A review of recent developments concerning the structure, mechanics and fluid flow  
350 properties of fault zones. *Journal of Structural Geology*, 32(11), 1557–1575.



- 351 Finley, R. J., Frailey, S. M., Leetaru, H. E., Senel, O., Couëslan, M. L., & Scott, M. (2013). Early  
352 operational experience at a one-million tonne CCS demonstration project, Decatur, Illinois,  
353 USA [Publisher: Elsevier]. *Energy Procedia*, *37*, 6149–6155.
- 354 Freiburg, J., Morse, D. G., Leetaru, H. E., Hoss, R. P., & Yan, Q. (2014). A depositional and  
355 diagenetic characterization of the Mt. Simon sandstone at the Illinois Basin-Decatur Project  
356 carbon capture and storage site, Decatur, Illinois, USA [Publisher: Illinois State Geological  
357 Survey, Prairie Research Institute, University of ...].
- 358 Furre, A.-K., Eiken, O., Alnes, H., Vevatne, J. N., & Kiær, A. F. (2017). 20 years of monitoring  
359 CO<sub>2</sub>-injection at Sleipner [Publisher: Elsevier]. *Energy procedia*, *114*, 3916–3926.
- 360 Furre, A.-K., Kiær, A., & Eiken, O. (2015). CO<sub>2</sub>-induced seismic time shifts at Sleipner [Pub-  
361 lisher: Society of Exploration Geophysicists and American Association of Petroleum ...].  
362 *Interpretation*, *3*(3), SS23–SS35.
- 363 Gasda, S. E., Bachu, S., & Celia, M. A. (2004). Spatial characterization of the location of potentially  
364 leaky wells penetrating a deep saline aquifer in a mature sedimentary basin. *Environmental*  
365 *geology*, *46*, 707–720.
- 366 Gassmann, F. (1951). Über die elastizität poröser medien: Vierteljahrsschrift der Naturforschenden  
367 Gesellschaft in Zurich, vol. 96.
- 368 Gilmore, K. A., Sahu, C. K., Benham, G. P., Neufeld, J. A., & Bickle, M. J. (2022). Leakage dynamics  
369 of fault zones: Experimental and analytical study with application to CO<sub>2</sub> storage. *Journal*  
370 *of Fluid Mechanics*, *931*, A31. <https://doi.org/10.1017/jfm.2021.970>
- 371 Grude, S., Landrø, M., & Osdal, B. (2013). Time-lapse pressure–saturation discrimination for CO<sub>2</sub>  
372 storage at the Snøhvit field [Publisher: Elsevier]. *International Journal of Greenhouse Gas*  
373 *Control*, *19*, 369–378.
- 374 Hale, D. (2013). Dynamic warping of seismic images: *Geophysics*, *78*. S105–S115.
- 375 Han, D., & Batzle, M. (2014). FLAG fluid calculator. *University of Houston Fluids/DHI Consortium*.
- 376 Hansen, O., Gilding, D., Nazarian, B., Osdal, B., Ringrose, P., Kristoffersen, J.-B., Eiken, O., &  
377 Hansen, H. (2013). Snøhvit: The history of injecting and storing 1 mt co<sub>2</sub> in the fluvial  
378 tubåen fm. *Energy Procedia*, *37*, 3565–3573.
- 379 Ivandic, M., Juhlin, C., Lueth, S., Bergmann, P., Kashubin, A., Sopher, D., Ivanova, A., Baumann,  
380 G., & Hennings, J. (2015). Geophysical monitoring at the Ketzin pilot site for CO<sub>2</sub> stor-  
381 age: New insights into the plume evolution [Publisher: Elsevier]. *International Journal of*  
382 *Greenhouse Gas Control*, *32*, 90–105.

- 383 Johnston, D. H. (2013). *Practical applications of time-lapse seismic data*. Society of Exploration  
384 Geophysicists.
- 385 Jung, N.-H., Han, W. S., Watson, Z., Graham, J. P., & Kim, K.-Y. (2014). Fault-controlled co2 leak-  
386 age from natural reservoirs in the colorado plateau, east-central utah. *Earth and Planetary  
387 Science Letters*, *403*, 358–367.
- 388 Kang, M., Christian, S., Celia, M. A., Mauzerall, D. L., Bill, M., Miller, A. R., Chen, Y., Conrad,  
389 M. E., Darrah, T. H., & Jackson, R. B. (2016). Identification and characterization of high  
390 methane-emitting abandoned oil and gas wells. *Proceedings of the National Academy of  
391 Sciences*, *113*(48), 13636–13641.
- 392 Krevor, S., de Coninck, H., Gasda, S. E., Ghaleigh, N. S., de Gooyert, V., Hajibeygi, H., Juanes,  
393 R., Neufeld, J., Roberts, J. J., & Swennenhuis, F. (2023). Subsurface carbon dioxide and  
394 hydrogen storage for a sustainable energy future [Publisher: Nature Publishing Group UK  
395 London]. *Nature Reviews Earth & Environment*, 1–17.
- 396 Lahann, R., Rupp, J., Medina, C., Carlson, G., & Johnson, K. (2017). State of stress in the illinois  
397 basin and constraints on inducing failure. *Environmental Geosciences*, *24*(3), 123–150.
- 398 Landrø, M., & Stammeijer, J. (2004). Quantitative estimation of compaction and velocity changes  
399 using 4D impedance and travelttime changes [Publisher: Society of Exploration Geophysi-  
400 cists]. *Geophysics*, *69*(4), 949–957.
- 401 Leetaru, H., & Freiburg, J. T. (2014). Litho-facies and reservoir characterization of the Mt  
402 Simon Sandstone at the Illinois Basin–Decatur Project [Publisher: Wiley Online Library].  
403 *Greenhouse Gases: Science and Technology*, *4*(5), 580–595.
- 404 MacBeth, C., Amini, H., & Izadian, S. (2020). Methods of measurement for 4D seismic post-stack  
405 time shifts [Publisher: Wiley Online Library]. *Geophysical Prospecting*, *68*(9), 2637–2664.
- 406 MacBeth, C., Mangriotis, M.-D., & Amini, H. (2019). Post-stack 4D seismic time-shifts: Inter-  
407 pretation and evaluation [Publisher: European Association of Geoscientists & Engineers].  
408 *Geophysical Prospecting*, *67*(1), 3–31.
- 409 MacBeth, C., & Izadian, S. (2023). A review and analysis of errors in post-stack time-shift inter-  
410 pretation [Publisher: European Association of Geoscientists & Engineers]. *Geophysical  
411 Prospecting*, *71*(8), 1497–1522.
- 412 Miocic, J. M., Gilfillan, S. M., Roberts, J. J., Edlmann, K., McDermott, C. I., & Haszeldine, R. S.  
413 (2016). Controls on co2 storage security in natural reservoirs and implications for co2 storage  
414 site selection. *International Journal of Greenhouse Gas Control*, *51*, 118–125.

415 Nordbotten, J. M., Kavetski, D., Celia, M. A., & Bachu, S. (2009). Model for co2 leakage including  
416 multiple geological layers and multiple leaky wells. *Environmental science & technology*,  
417 *43*(3), 743–749.

418 Onishi, T., Nguyen, M. C., Carey, J. W., Will, B., Zaluski, W., Bowen, D. W., Devault, B. C.,  
419 Duguid, A., Zhou, Q., Fairweather, S. H., et al. (2019). Potential co2 and brine leakage  
420 through wellbore pathways for geologic co2 sequestration using the national risk assessment  
421 partnership tools: Application to the big sky regional partnership. *International Journal of*  
422 *Greenhouse Gas Control*, *81*, 44–65.

423 Pörtner, H., Roberts, D. C., Poloczanska, E., Mintenbeck, K., Tignor, M., Alegría, A., Craig, M.,  
424 Langsdorf, S., Löschke, S., Möller, V., et al. (2022). IPCC, 2022: Summary for policymakers  
425 [Publisher: Cambridge University Pres].

426 Ringrose, P., Andrews, J., Zweigel, P., Furre, A.-K., Hern, B., & Nazarian, B. (2022). Why ccs is  
427 not like reverse gas engineering. *First Break*, *40*(10), 85–91.

428 Roach, L. A., & White, D. (2018). Evolution of a deep co2 plume from time-lapse seismic imaging  
429 at the aquistore storage site, saskatchewan, canada. *International Journal of Greenhouse*  
430 *Gas Control*, *74*, 79–86.

431 Santos, J. M., Davolio, A., MacBeth, C., & Schiozer, D. J. (2016). 4D seismic interpretation of the  
432 Norne Field—a semi-quantitative approach [Issue: 1]. *78th EAGE Conference and Exhibition*  
433 *2016, 2016*, 1–5.

434 Stork, C. (2020). How does the thin near surface of the earth produce 10–100 times more noise on  
435 land seismic data than on marine data? *First Break*, *38*(8), 67–75.

436 Strandli, C. W., & Benson, S. M. (2013). Identifying diagnostics for reservoir structure and co2  
437 plume migration from multilevel pressure measurements. *Water Resources Research*, *49*(6),  
438 3462–3475.

439 Strandli, C. W., Mehnert, E., & Benson, S. M. (2014). Co2 plume tracking and history matching  
440 using multilevel pressure monitoring at the illinois basin–decatour project. *Energy Procedia*,  
441 *63*, 4473–4484.

442 Swager, L. (2019). *ADM CCS1 Injection Well Mechanical Integrity Report March 2019 Pulsed*  
443 *Neutron eXtreme* (tech. rep.).

444 Yang, Z., Xu, T., Wang, F., Yang, Y., Li, X., & Zhao, N. (2018). Impact of inner reservoir faults  
445 on migration and storage of injected co2. *International Journal of Greenhouse Gas Control*,  
446 *72*, 14–25.

- 447 Zaluski, W., & Lee, S.-Y. (2021). *2020 IBDP Final Static Geological Model Development and*  
448 *Dynamic Modelling* (tech. rep.).
- 449 Zhang, L., Yang, Q., Zhang, S., Shan, L., Jiang, Q., & Sun, M. (2024). Enhanced co2 storage  
450 efficiency due to the impact of faults on co2 migration in an interbedded saline aquifer.  
451 *International Journal of Greenhouse Gas Control*, 133, 104104.